Proceedings of the Mustansiriyah International Conference on Applied Physics (MICAP-2021)

Cellulose–Fe_2O_3 Nanocomposites for Removal of Cu(II) and Cd(II) Ions in Aqueous Medium

Randa K. Hussain, Wisam J. Aziz* and Asaad M. Abbas

College of Science, Physics Department, Mustansiriyah University, Palestine St., 10052, Baghdad, Iraq

Doi: 10.12693/APhysPolA.140.311 *e-mail: wisamj.aziz@uomustansiriyah.edu.iq

Fe_2O_3 nanoparticles were synthesized by thermal hydrolysis. A cellulose–Fe_2O_3 nanocomposite was extracted from the peels of mandarin citrus fruit using cellulose as a reducing agent. Small, uniformly distributed crystals were obtained at 60°C, pH 8, for the reaction time of 1 h. The physical properties of the samples were analyzed using X-ray diffraction, field emission scanning electron microscope, and a vibrating-sample magnetometer. The Fe_2O_3 nanoparticles were spherical and uniformly distributed bounded with the fibrous cellulose, the particle size ranged from 28.21 to 35.91 nm. The cellulose–Fe_2O_3 nanocomposite exhibited a superparamagnetic behavior, while the Fe_2O_3 nanoparticle demonstrated a ferromagnetic effect. The nanocomposite showed high adsorption capacity after removing Cu(II) and Cd(II) ions from water.

topics: cellulose–Fe_2O_3 composite, metal–ion removal, super-paramagnetic

1. Introduction

Metallic nanoparticles (NPs) have garnered significant attention for their properties and broad applications, including catalysts [1], biosensors [2], drug delivery systems, pollution purification [3], and dye removal [4]. In many studies, nanoparticles were synthesized by standard physico-chemical processes, but recently, biosynthetic methods are increasingly utilized. The use of organisms in nanotechnology has advanced rapidly due to the simplicity of obtaining nanoparticles and significantly reduced the impact on the environment as no toxic chemical compounds are produced.

Metal nanoparticles are successfully prepared from many natural sources, such as plants, or synthesized using bacteria [5, 6] and fungi [7, 8]. Extraction of nanoparticles from plants allows to obtain higher molecular masses than by other biological methods, and it is free from the potential biohazards of using bacteria and fungi. The biological source and the preparation conditions have a significant effect on the morphology and properties of the produced nanoparticles. Iron nanoparticles (Fe_2O_3 NPs) with a 50 nm diameter have an amorphous structure when prepared by extraction from sorghum aqueous solution at room temperature. These nanoparticles are suitable for environmental waste treatment [9]. Fe_2O_3 have a hexagonal structure and exhibit paramagnetic behavior. The elemental composition of the energy dispersive spectrum (EDS) revealed impurities of chloride ions, phosphorus, and oxygen, the latter two of which may appear due to oxidation at the surface of the sample. Fe_2O_3 NPs have been successfully extracted under a variety of conditions from many plants, including *Lawsonia inermis*, *Gardenia*, jasminoides, green tea, and *Azadirachta* [10–12].

The reaction temperature and pH are the controlling factors of the morphology and size of the generated particles, and temperatures of 70–80°C, and a wide range of pHs have been demonstrated as suitable for Fe NP extraction. Spheroid nanoparticles were synthesized through a one step bioroute using eucalyptus leafs at ambient temperature [13]. The Fourier transform infrared (FTIR) spectroscopy techniques showed the presence of polyphenols bonded to the surfaces of Fe_2O_3 NPs as a capping/stabilizing agent [14]. The X-ray diffraction (XRD) pattern revealed the presence of iron oxide, iron oxyhydroxide inermis, and Fe_2O_3NPs, in the reduction of green tea [15, 16]. Magnetic Fe_3O_3 nanoparticles were synthesized via green methods by the reduction of $FeCl_3$ solution utilizing an aqueous seaweed solution as a stabilizing and metal reducing agent.

The metallurgy of iron-based coke and coal as sources of reducing effects include CO_2 gas emissions into our environment. The development of new, efficient green technologies based on the

reducing effect of renewable, abundant sources has become critical. Such green technologies should replace technologies based on coke and coal and lead to further development in this field [17]. The oxidizing agent, such as many types of metal catalysts, could generate oxidized cellulose with the assistance of some chemical groups, such as hydroxyl, present in the cellulose structure. In this work, for the first time, cellulose is assessed for its potential to reduce iron oxides. Cellulose is a natural polymer that is easily available, renewable, degradable, and low-cost. It is available on land and is present in the plant cell walls as a combination with hemicellulose, lignin, waxes, and other compounds [18].

Cellulose microfibrils can be extracted from their natural sources by chemical and mechanical methods, depending on the cellulose source. The length of the produced fiber can range from nanometers to micrometers with a diameter of 5–10 nm [19, 20]. Chemically, cellulose ($C_6H_{10}O_5$) has monomer units connected by $\beta(1 \to 4)$-glycosidic bonds. The crystal size and spatial arrangement of molecules are converted to another form of polymorph arrangement depending on the specific cellulose source and the isolation method. The $\beta(1 \to 4)$-glycosidic bond imparts on the cellulose poor solubility, and makes it insoluble in water and common organic solvents [21].

The aim of this research is to prepare and study the properties of Fe oxide nanoparticles using plant extraction in a one-step procedure in which cellulose is utilized as a stabilizer/reduction agent. This method can be preventing of carbonated cellulose encapsulated with Fe oxide nanoparticles. In this article, ion removal nanocomposites synthesized in simple, cheap, and recycling materials based on green metal extraction methods are proposed. We select the iron oxide mixed with the cellulose which is also biological resource and together they formed a green composite that could be safely used in water treatment applications.

2. Experimental procedure

Peels of the mandarin citrus fruits were cleaned and dried at room temperature. The sample was prepared by mixing 30 g of powdered peels with 50 ml distilled water, and the aqueous solution was boiled at 90°C. To obtain a pure mandarin extract, the aqueous solution was filtered. The amount of 1 g of iron nitrate ($Fe(NO_3)_3 \cdot 9H_2O$), the reducing agent, was dissolved into 20 ml distilled water. The solution was stirred at 60°C for 15 min, then 30 ml mandarin extract was added to the iron nitrate solution, and the temperature increased to (60°C or 90°C). The Fe oxide nanoparticle formation was primarily indicated by color change, then 30 g of cellulose $(C_6H_{10}O_5)_n$, an additional reducing agent [22], was added. The solution pH 8 was controlled by adding 1 M of NaOH. The aqueous solution was carefully mixed and kept on a hot plate for 1 h. The solution change of color from yellow to dark brown indicated the presence of iron in the solution. The extracted material was filtered and washed many times using pure ethanol and water to remove any residual materials from the sample. Finally, the extracted composite was dried at room temperature for 24 h.

3. Results and discussions

The reduction mechanism has two stages. Firstly the −OH phenol of circuit extraction bond is broken to a complex partial bond of Fe^{3+}. The second stage is the fracture of the partial bond forming electrons that help to reduce the Fe ions to nanoparticles and obtain oxidation [23]

$$n\mathrm{Fe}^{3+} + 3\big(\mathrm{Ar}{-}(\mathrm{OH})_n\big) \rightarrow$$

$$n\mathrm{Fe}^{0} + 2n\big(\mathrm{Ar}{=}\mathrm{O}\big) + 2n\mathrm{H}^{+}, \qquad (1)$$

where Ar is the phenyl group, and n is the number of hydroxyl groups oxidized by Fe^{3+}.

To investigate the crystalline structure, the cellulose Fe-oxide composite samples were characterized by XRD. The spectral analysis showed the presence of the composites (see Fig. 1). Cellulose is present in two distinct phases I-alpha (in a triclinic crystal structure) and I-beta (in a monoclinic crystal structure), and the amount of each phase depends on the cellulose source. The XRD pattern is shown in Fig. 1. The main cellulose bands at $2\theta = 15.0°$, 22.6°, and 34.6° are due to (101), (002), and (040), respectively.

The general XRD patterns indicated that the cellulose pattern was retained even after being loaded with the Fe oxide particles. However, the main peaks of a metallic oxide nanoparticle appeared at $2\theta = 29.4°$, 39.4°, and 57.4°. The XRD patterns revealed that the nano Fe_2O_3 was produced in two phases: the sharp peak belongs to (220), reflecting predominantly the γ-Fe_2O_3, while α-Fe_2O_3 was demonstrated by (113) and (024). Table I shows the XRD data for the strongest peaks of Fe oxide. At 90°C, these peaks tended to vanish, indicating the predominance of γ-Fe_2O_3 (see Fig. 1b, c). This

TABLE I

XRD data for strongest peaks of Fe_2O_3.

Sample	XRD 2θ [°]	(hkl)	FWHM [°]
Fe_2O_3 NPs	15.0	(101)	0.16
	22.6	(002)	0.170
	34.6	(040)	0.118
Fe_2O_3–cellulose at 60°C	29.3	(220)	0.117
	38.8	(113)	0.118
	57.4	(024)	0.155
Fe_2O_3–cellulose at 90°C	29.3	(220)	0.117

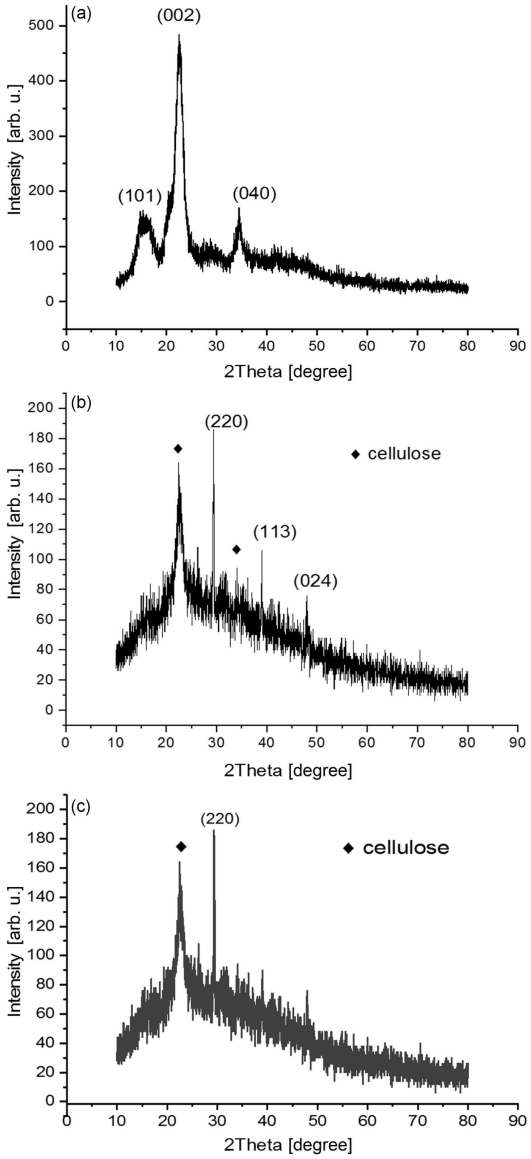

Fig. 1. XRD pattern for: (a) pure cellulose, (b) Fe_2O_3–cellulose at 60°C, (c) Fe_2O_3–cellulose at 90°C.

spectral analysis is consistent with results achieved by [23] that extracted nano Fe_2O_3 from citrus fruits. The patterns measured by the XRD technique were adjusted to be close to the cellulose pattern. The iron oxide hybrid with organic materials consisted of a glucose group, and the nanoparticles of Fe_2O_3 exfoliated the upper layer of a glucose group due to the attraction between them [24]. In this work, the interaction of nano Fe_2O_3 with cellulose surface was successfully achieved.

The spherical shaped crystals, placed on cellulose, conserved their spherical-fiber crystal phase properties, similar to that in the previous study [17]. The high-intensity peak at 29.4° indicated an increase in crystallinity. This influence is attributed to the change in temperature and pH, and iron oxide morphology did not change in time.

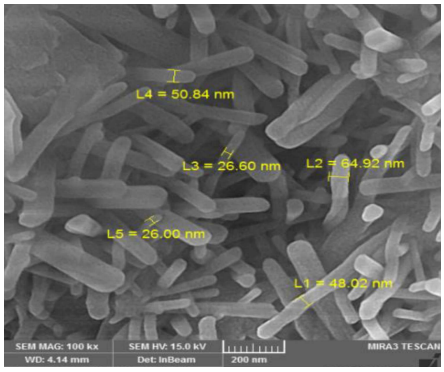

Fig. 2. FESEM images of cellulose fibers.

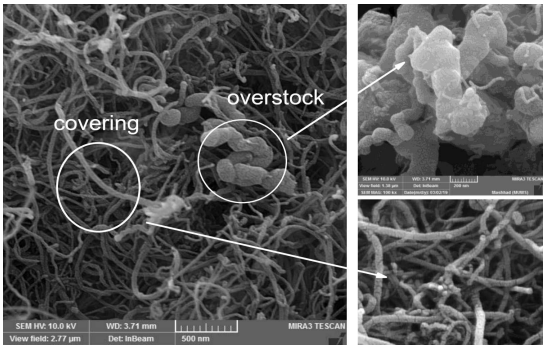

Fig. 3. FESEM images of cellulose–Fe_2O_3 at 60°C.

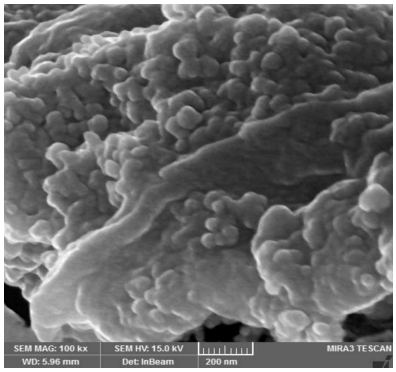

Fig. 4. FESEM images of cellulose–Fe_2O_3 at 90°C.

The FESEM images (see Fig. 2) show a homogeneous fibrous morphology of cellulose, the diameter of fibers was 26–64 nm. These fibers appear loaded with iron oxide nanoparticles that localized on the cellulose surface as cellulose/Fe_2O_3 composites.

In Fig. 3, the two distinctive loadings appear in FESEM cellulose–Fe_2O_3, nanoparticles fully and smoothly covered the fiber, which is the general situation, especially at 60°C. In some locations, however, the nanoparticles seemed to overstock on the cellulose fiber.

The overstocking was more pronounced at 90°C, and the surface of the composite had clusters with a specific shape (see Fig. 4).

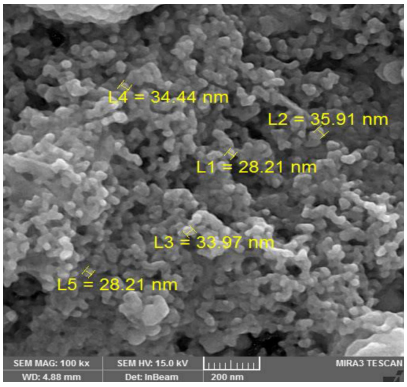

Fig. 5. Particles size of Fe_2O_3–cellulose at 60°C dedicated by FESEM.

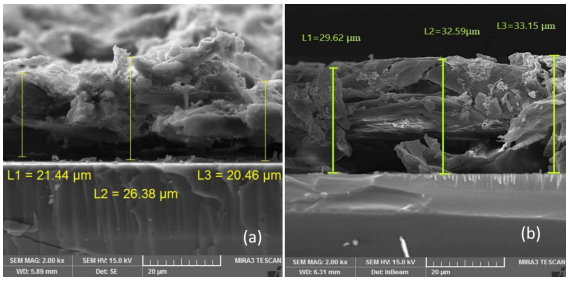

Fig. 6. FESEM cross-sectional images of: (a) Fe_2O_3–cellulose at 60°C and (b) Fe_2O_3–cellulose at 90°C.

The smooth surface of cellulose fiber changed after it was loaded with nanoparticles, and the obtained crystal size was 38–44 nm for cellulose/Fe_2O_3 prepared at 60°C (see Fig. 5). Moreover, smaller and uniformly spherical shaped particles capsulated the cellulose fibers and formed a uniform coating at 60°C. The nanoparticles coating the net of cellulose fibers demonstrated good dispersion onto the matrix with uniform size of these nanoparticles.

Moreover, it was observed in Fig. 6 that the cross-sectional thickness and the grain size could be modified according to the temperature of the synthesis.

The nanoparticles prepared at 90°C acquired a larger size. They produced a thicker coating of uniform spherical particles accumulating onto a cellulose fiber. Also, the figure shows nanoholes with a uniform distribution.

The magnetic properties were characterized by vibrating sample magnetometer (VSM), and Fig. 7 shows the M–H curves of Fe_2O_3 nanopowder and cellulose/Fe_2O_3 composites. The hysteresis loops confirm the magnetic behavior, whereas the M–H curve for Fe_2O_3 nanopowder demonstrated weak ferromagnetic behavior. As seen in Fig. 8a, the sugariness ratio (M_r/M_s) was calculated to be 0.02, creating a square loop shape, whereas the cellulose–Fe_2O_3 composites had narrow hysteresis loops. In cellulose–Fe_2O_3 composites, the superparamagnetic behavior has two criteria: magnetic saturation and residual magnetization. Nanoparticles are required

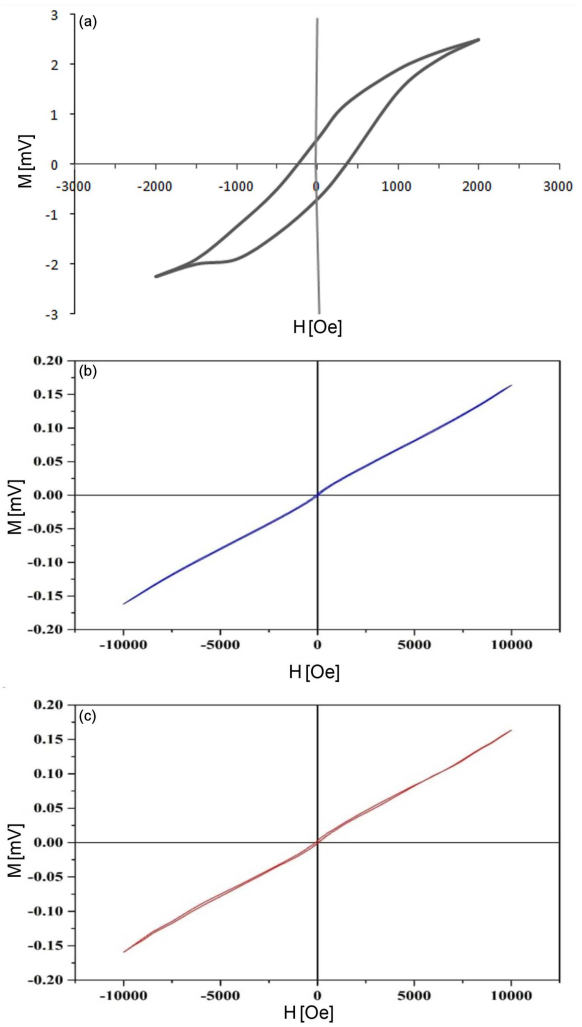

Fig. 7. The magnetization curves of: (a) Fe_2O_3 NPs, and cellulose–Fe_2O_3 at (b) 60°C and (c) 90°C.

to apply a high external magnetic field to reach the magnetic saturation, while they rapidly lose their magnetization after removing the external magnetic field, and the remnant magnetization becomes close to zero. In our case, these criteria were met (cellulose–Fe_2O_3 lost the magnetic behavior and returned to its original state after the external magnetic field was removed). The domain relaxation process became very fast when the reduced domain size became comparable with crystal size.

The reduction in the size scale also led to a decrease of the magnetic coercivity (H_c). In cellulose–Fe_2O_3 prepared at 60°C, which had smaller crystal size of Fe_2O_3 particles, the size effect became more pronounced and the coercivity approached zero. Using the cellulose matrix changed the behavior of Fe_2O_3 nanoparticles from weak ferromagnetic (see Fig. 7a) to superparamagnetic behavior with a smaller coercivity as smaller crystals. Clearly the residual magnetization effect almost vanished in the sample synthesized at 90°C (see Fig. 7b and c). Table II lists the magnetic values of iron oxide nanoparticles and their composites.

TABLE II

Remnant magnetization, magnetic saturation, magnetic coercivity and sugariness ratio.

Sample	M_r [mV]	M_s [mV]	H_c [Oe]	M_r/M_s ratio
Fe_2O_3 NPs	0.5	2.5	500	0.20
Fe_2O_3–cellulose at 60°C	0.0001	0.17	64	0.0005
Fe_2O_3–cellulose at 90°C	0.0016	0.158	123	0.0101

The magnetic properties of Fe_2O_3 NPs motivated the creation and use of this nanocomposite to remove cadmium ions (Cd(II)) and copper ions (Cu(II)) from contaminated water. The removal mechanism is based on the adsorption of contaminating ions present in water onto the nanocomposite surface assisted by magnetic behavior. Adsorption was measured by suspending 0.05 g Fe_2O_3/cellulose (at 60°C) in 10 mg/l of Cd(II), and Cu(II) in distilled water. The adjusted pH of 6 was maintained, with stirring, at room temperature for 2 h. The concentrations of Cd(II) and Cu(II) were measured by mass spectroscopy before and after Fe_2O_3–cellulose was added to the mixture. The adsorption efficiency (Adsor in [%]) was determined accordingly using

$$\text{Adsor} = \frac{C_\text{i} - C_\text{f}}{C_\text{i}} \times 100, \tag{2}$$

where C_i and C_f are the initial and final concentrations, respectively, of ions in distilled water. The adsorption efficiency led to high percentage of metal ion removal 87.4% and 82.8% for Cu(II) and Cd(II) ions, respectively.

4. Conclusions

Pure and crystalline iron oxide nanoparticles were effectively produced from mandarin citrus via green synthesis with a sustained cellulose reducing agent *in situ* approach. The obtained NPs displayed ferromagnetic properties, while their composite with cellulose showed superparamagnetic properties with $0.0005 M_r/M_s$ ratio. Also the interaction of nanoparticles of Fe_2O_3 with cellulose surface was successfully achieved. Uniform distribution of spherical NPs on the fibrils cellulose nanocomposite showed good morphologic effects that provided high adsorption efficiencies of Cu(II) and Cd(II) reaching to 87.4% and 82.8%, respectively, removing the ions from water.

References

[1] M. Nasrollahzadeh, S.M. Sajadi, A. Rostami-Vartooni, M. Khalaj, *J. Mol. Catal. A* **396**, 31 (2015).

[2] A.A. Ensafi, N. Ahmadi, B. Rezaei, *Sens. Actuat. B* **239**, 807 (2017).

[3] S.F. Sweeney, G.H. Woehrle, J.E. Hutchison, *J. Am. Chem. Soc.* **128**, 3190 (2006).

[4] T. Shahwan, S.A. Sirriah, M. Nairat et al., *Chem. Eng. J.* **172**, 258 (2011).

[5] S. He, Z. Guo, Y. Zhang, S. Zhang, J. Wang, N. Gu, *Mater. Lett.* **61**, 3984 (2007).

[6] A.R. Shahverdi, S. Minaeian, H.R. Shahverdi, H. Jamalifar, A.A. Nohi, *Process. Biochem.* **42**, 919 (2007).

[7] Z. Sadowski, I. Maliszewska, B. Grochowalska, I. Polowczyk, T. Kozlecki, *Mater. Sci. Poland* **26**, 419 (2008).

[8] A. Syed, S. Saraswati, G.C. Kundu, A. Ahmad, *Spectrochim. Acta A* **114**, 144 (2013).

[9] E.C. Njagi, H. Huang, L. Stafford, H. Genuino, H.M. Galindo, J.B. Collins, G.E. Hoag, S.L. Suib, *Langmuir* **27**, 264 (2011).

[10] S. Machado, S. Pinto, J. Grosso, H. Nouws, J.T. Albergaria, C. Delerue-Matos, *Sci. Tot. Environm.* **445**, 1 (2013).

[11] L. Huang, X. Weng, Z. Chen, M. Megharaj, R. Naidu, *Spectrochim. Acta A* **130**, 295 (2014).

[12] T. Naseem, M.A. Farrukh, *J. Chem.* **20**, 15 (2015).

[13] Q. Lu, Y. Zhang, H. Hu, W. Wang, Z. Huang, D. Chen, M. Yang, J. Liang, *Nanomaterials* **9**, 275 (2019).

[14] T. Wang, X. Jin, Z. Chen, M. Megharaj, R. Naidu, *Sci. Tot. Environm.* **466**, 210 (2014).

[15] D. Guo, L. Zhu, S. Guo et al., *Fuel Process. Technol.* **148**, 276 (2016).

[16] R. Hussain, W. Aziz, I. Abbas Ibrahim, *J. Nanostruct.* **9**, 761 (2019).

[17] A.P. Mathew, K. Oksman, M. Sain, *J. Appl. Polym. Sci.* **97**, 2014 (2005).

[18] A.N. Frone, D.M. Panaitescu, D. Donescu, C.I. Spataru, C. Radovici, R. Trusca, R. Somoghi, *BioResources* **6**, 487 (2011).

[19] H. Leipner, S. Fischer, E. Brendler, W. Voigt, *Macromol. Chem. Phys.* **201**, 2041 (2000).

[20] I.A. Ibrahim, R.K. Hussain, W.J. Aziz, *AIP Conf. Proc.* **2213**, 020019 (2020).

[21] L. Johnson, W. Thielemans, D.A. Walsh, *Green Chem.* **13**, 1686 (2011).

[22] H.R. Ali, H.N. Nassar, N.S. El-Gendy, *Energy Sourc. A* **39**, 1425 (2017).

[23] S.A. Ogundare, W.E. van Zyl, *Surf. Interfaces* **13**, 1 (2018).

[24] G. Orfanakis, M. Patila, A.V. Catzikonstantinou et al., *Front. Mater.* **5**, 25 (2018).